Bakker A., Van den Akker H.E.A. (1994) Single-Phase Flow in Stirred Reactors. Chemical Engineering Research and Design, TransIChemE Vol. 72, Number A4, July 1994, page 583-593.

SINGLE-PHASE FLOW IN STIRRED REACTORS

A. BAKKER and H. E. A. VAN DEN AKKER

Kramers Laboratorium voor Fysische Technologie, Delft University of Technology, Delft, The Netherlands

Single-phase flow patterns in stirred reactors were investigated both computational, with FLUENT, and experimental, by Laser Doppler Velocimetry (LDV). This was done for three different impeller types, viz. two axial flow impellers and a disc-turbine. The effect of geometrical modifications to the vessel geometry was studied as well. In particular, the exact baffle arrangement has a strong impact on the flow pattern. It will be shown that the single-phase flow patterns exhibit unexpected features not recognized before.

An accurate numerical computation requires full three dimensional grids. Further, anisotropic turbulence models, in this case the Algebraic Stress Model, give better predictions than the k-ε turbulence model. When these requirements are met, the predicted flow patterns compare very well with the experimental data. Thus, a quick assessment of the influence of geometrical variables can be made just using numerical simulations.

Keywords: mixing; agitation; impeller; flow field; laser Doppler; Computational Fluid Dynamics

INTRODUCTION

In this paper the single-phase flow in stirred vessels is described. One of the conclusions from the work of Bakker and Van den Akker[1] and Bakker[2] is that it is difficult to get insight in the processes in a gassed stirred tank by investigating overall quantities. The description of the single-phase flow in the stirred vessel given here, can serve as a starting point for modelling the local gas-liquid flow in the tank[3].

Since experimental velocity and turbulence measurements are time consuming and not always possible, the single-phase flow patterns are studied by means of calculations performed with the general fluid flow code FLUENT. One of the advantages of this method is that the amount of information which can be generated by such calculations is far larger than what can be reached generally by performing experiments. For example, FLUENT calculates all the turbulence properties throughout the flow field, including all the Reynolds stresses and the energy dissipation rate, something which is virtually impossible to achieve by LDV experiments.

In this paper, the influence of grid size, turbulence modelling and numerical techniques on the computational results are studied by comparing various standard cases with experimental velocity measurements. Three different impellers are used, a disc-turbine, an A315 hydrofoil impeller and a pitched blade turbine.

LITERATURE

Developments in the field of Computational Fluid Dynamics (CFD) have led to an increased interest in the numerical computation of flow field in stirred tank reactors, starting with Harvey and Greaves[4,5]. These authors modelled the flow generated by a disc turbine on a two-dimensional grid. Although their results had a qualitative appeal, they did not compare very well with literature data. Later on, Placek *et al.*[6,7] also modelled the flow in a turbine stirred tank using a modified three-equation k-ε model. Their results showed a reasonable extent of agreement with velocity measurements near the vessel wall, performed with a pitot tube. Pericleous and Patel[8] modelled the flow with a disc turbine as well as the flow with axial flow impellers. Due to the use of a simple one-equation turbulence model, their velocity calculations had a limited accuracy only.

Middleton *et al.*[9] were the first to present full 3-dimensional computations of the flow in a turbine stirred tank in the open literature. These authors also used the calculated single-phase flow patterns as a basis for predicting the chemical reaction yield in such vessels. Ranade and Joshi[10–13] published an interesting series of papers about the single-phase flow in vessels equipped with disc turbines and several types of pitched blade turbines. They presented extensive data sets of velocity measurements done with an LDV system, and performed a large series of flow computations done with an in-house code. Hutchings *et al.*[14] used FLUENT for flow predictions in vessels equipped with disc turbines and Lightnin A315 impellers. For the disc turbine, the predicted flow patterns compared quite well with the experimental data. Due to the fact that the computations for the A315 were done on a two-dimensional grid instead of on a full 3-dimensional grid, the predicted flow patterns for this impeller did not compare too well with the experimental data. Kresta and Wood[15] presented a model for the turbulent kinetic energy and the turbulent energy dissipation rate at the vertical swept boundary of a disc turbine. They reported that their calculations with FLUENT gave a good prediction of the behaviour of

0263-8762/94/$05.00+0.00

the turbulent kinetic energy and its dissipation rate in the discharge zone of the impeller.

All the authors mentioned above performed their calculations using isotropic turbulence models, mostly the k-ε model. The turbulence in a stirred vessel is, however, far from isotropic. Apart from anisotropic turbulence generation due to the strong rotational character of the flow, the flow is periodic, due to the fact that the impeller blades pass the baffles. Van't Riet *et al.*[16] pointed out that this results in periodic velocity fluctuations, a phenomenon called pseudo-turbulence. It may be clear that the best simulation results are to be expected when time-dependent calculations are done, in combination with the use of an anisotropic turbulence model. Unfortunately this is far beyond current computational capabilities.

Placek *et al.*[7] therefore proposed a three equation k-ε model, which regards the pseudo turbulence as isotropic turbulence of a different length and time scale. This approach was not followed here, but it is clear that the kinetic energy of the pseudo turbulence in the outflow of the impeller should be included in the boundary conditions. To account for the anisotropy of the turbulence in the flow field, the Algebraic Stress Model[17,18] was used for modelling the Reynolds stresses.

EXPERIMENTAL

Since CFD has not yet reached the stage in which the calculated flow patterns can always be regarded as correct without any experimental validation, there remains a need for experimental velocity data. Further, for fluid flow calculations in a stirred tank, experimentally determined impeller boundary conditions are needed.

Therefore, a series of velocity measurements were performed with a two-dimensional TSI fiberflow laser-doppler system. The system incorporates two TSI-IFA550 flow analysers, a 4W Argon-Ion laser from Spectra-Physics and a 80386 MS-Dos computer. Data acquisition and data analysis were performed with TSI-Find software.

For fast data acquisition the system was operated in the random sampling mode rather than in the even time sampling mode. From the velocity data gathered in this way, histograms were constructed and the first and second moments were calculated.

The velocity measurements were performed in a plexiglass stirred tank, being 0.444 m in diameter and filled with distilled water at room temperature. The liquid surface was free. The vessel was equipped with four baffles with a width $W = 0.077\ T$ and mounted at a distance of $0.023\ T$ ($= 10$ mm) from the wall. The torque exerted by the impeller was measured with a Vibro-meter torque transducer, mounted in the shaft.

It is known that the flow in a stirred vessel is not fully stationary but contains high frequency periodicities due to the rotation of the impeller. This could not be taken into account and all experimental velocity and turbulence data presented here are time averages including this so-called pseudo turbulence.

Axial velocities could be measured without a problem, but due to refraction on the round vessel wall, determining the position of the measurement volume for the tangential velocities was a laborious task. Further, due to the fact that the measurement volumes for the axial velocity and for the tangential velocity did not have the same position, Reynolds stresses could not be measured. As a result of these experimental problems, tangential velocities and axial velocities, together with their fluctuations, were only measured in the outflow of the impeller to generate impeller boundary conditions. For validation of the predicted flow patterns, however, only axial velocities were measured at various positions in the vessel. The experimental problems mentioned above can be overcome by placing the round vessel in a square tank, filled with water. However, such a tank was not available. In all cases studied, the impellers were mounted at an impeller to bottom clearance of $C = 0.3\ T$. The disc turbine (DT) was operated at $N = 3$ Hz, the A315 and the pitched blade turbine (PBT) were operated at $N = 6$ Hz. The diameter of the impellers was $D = 0.4\ T$ in all cases.

THEORY OF FLUID FLOW MODELLING

The flow fields in the stirred tank reported in this paper were calculated with the commercially available general purpose code FLUENT, version 2.99. FLUENT solves the fluid flow equations on a finite difference grid. All calculations are performed for incompressible steady-state flow. The time averaged continuity equation reads:

$$\vec{\nabla}.\vec{u} = 0 \tag{1}$$

Here $\vec{u}$ denotes the time averaged velocity vector, and $\vec{u}'$ the time dependent fluctuating velocity component. Further, the time-averaged momentum balance can be written as:

$$\vec{\nabla}.(\vec{u}\vec{u}) = -\vec{\nabla}.\left(\frac{p}{\rho}\vec{I}\right) + \vec{\nabla}.(\nu(\vec{\nabla}\vec{u} + (\vec{\nabla}\vec{u})^{\mathrm{T}})) - \vec{\nabla}.\overline{\vec{u}'\vec{u}'} \tag{2}$$

The first term on the right hand side of this equation denotes the divergence of the pressure, the second term is the divergence of the viscous stresses and the third term is the divergence of the Reynolds stress tensor.

Although exact balance equations for the Reynolds stress tensor can be derived, the set of equations is not closed due to the averaging process. Therefore the Reynolds stress tensor requires modelling. This can, for example, be done by using the so-called Boussinesq hypothesis, which models the Reynolds stresses as being proportional to the mean strain rate:

$$-\overline{\vec{u}'\vec{u}'} = -\tfrac{2}{3}k\vec{I} + \nu_t(\vec{\nabla}\vec{u} + (\vec{\nabla}\vec{u})^{\mathrm{T}}) \tag{3}$$

The turbulent viscosity ν_t depends on the turbulence structure only, and not on the fluid properties. In the k-ε model ν_t is calculated from:

$$\nu_t = c_\mu \frac{k^2}{\varepsilon} \tag{4}$$

The spatial distributions of the turbulent kinetic energy density k, defined as:

$$k = \tfrac{1}{2}\overline{\vec{u}'.\vec{u}'} \tag{5}$$

and of the turbulent energy dissipation rate density ε are calculated from their respective balance equations. The model equation for k reads:

$$\vec{u}.\vec{\nabla}k = \vec{\nabla}.((\nu + \nu_t/\sigma_k)\vec{\nabla}k) + P_k - \varepsilon \quad (6)$$

The model equation for ε is:

$$\vec{u}.\vec{\nabla}\varepsilon = \vec{\nabla}.((\nu + \nu_t/\sigma_\varepsilon)\vec{\nabla}\varepsilon) + c_{\varepsilon 1}\frac{\varepsilon}{k}P_k - c_{\varepsilon 2}\frac{\varepsilon^2}{k} \quad (7)$$

P_k denotes the production of k by the interaction with the mean strain rate:

$$P_k = -\overline{\vec{u}'\vec{u}'}:(\vec{\nabla}\vec{u}) \quad (8)$$

Further c_μ, σ_k, σ_ε, $c_{\varepsilon 1}$ and $c_{\varepsilon 2}$ are model constants. The k-ε model, however, has a limited validity only. Especially in flows with a strong swirl, this model is known to be inaccurate. This asks for the development of so-called Reynolds stress models, in which Reynolds stress balance equations are solved. These RSM models can be simplified by using the Rodi assumption,[17] which models the transport of the Reynolds stresses as being proportional to the transport of k. This leads to the so-called Algebraic Stress Model (ASM):

$$-\overline{\vec{u}'\vec{u}'} = \frac{2}{3}k\vec{I}\left[1 - \frac{(1-c_2)\dfrac{P_k}{\varepsilon}}{\dfrac{P_k}{\varepsilon} - (1-c_1)}\right] + \frac{1-c_2}{\dfrac{P_k}{\varepsilon} - (1-c_1)}\frac{k}{\varepsilon}(\vec{P} - \tfrac{2}{3}P_k\vec{I}) \quad (9)$$

$$\vec{P} = -(\overline{\vec{u}'\vec{u}'}.(\vec{\nabla}\vec{u}) + (\overline{\vec{u}'\vec{u}'}.(\vec{\nabla}\vec{u}))^T) \quad (10)$$

Here c_1 and c_2 are model constants. For reasons of comparison several flow computations were done with both the k-ε model and the ASM. The model constants for both the k-ε model and the ASM are given in Table 1.

THE COMPUTATIONAL MODEL

Impeller Boundary Conditions

Calculations were performed for a radially pumping disc turbine and for two axially pumping impellers, viz. an A315 and a standard pitched blade impeller with six blades.

There are several possibilities for modelling the impellers. For example, axial flow impellers can be modelled as a momentum source using airfoil theory[8]. The flow through a disc turbine, on the other hand can directly be calculated by modelling the turbine blades as being at rest while having the tank rotating[14]. One of the problems with this procedure is that now the baffles require modelling. These two methods, however, have not yet been proven to yield correct predictions. Further, it was not possible to incorporate these models in FLUENT 2.99. In later versions of FLUENT this is possible, but these were not available at the time of the research. Thus, in this work the impellers were modelled by prescribing experimental flow profiles as measured with the LDV system, in the outflow of the impeller.

Table 1. The model constants used in the turbulence modelling.

c_μ	σ_k	σ_ε	$c_{\varepsilon 1}$	$c_{\varepsilon 2}$	c_1	c_2
0.09	1.0	1.3	1.44	1.92	2.2	0.45

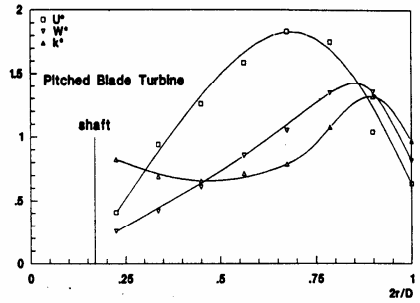

Figure 1. Velocity and turbulence profiles in the outflow of the pitched blade turbine, experimental data.

For the disc turbine the u, v, and w-velocities, denoting the axial, radial and tangential velocities respectively, together with the turbulent kinetic energy k and dissipation rate ε have been prescribed on the vertical swept boundary of the impeller, using parabolic profiles according to the data presented by Ranade and Joshi[12,13].

For the computations with the pitched blade impeller and the A315 impeller the velocity and turbulence profiles were prescribed at the bottom surface of the impellers, according to own experimental data, see Figure 1 for the PBT.

In the graphs all the mean velocities and k are made dimensionless with ($N\,Fl_1\,D$), which is proportional to the mean axial velocity in the impeller outflow:

$$u^* = \frac{u}{NFl_1D} \quad w^* = \frac{w}{NFl_1D} \quad k^* = \frac{\sqrt{2k}}{NFl_1D} \quad (11)$$

For the axial flow impellers the pumping number Fl_1 is defined as:

$$Fl_1 = \frac{Q_1}{ND^3} = \frac{1}{ND^3}\int_0^{D/2} u(z = H - C + H_i/2)2\pi r\,dr \quad (12)$$

H_i is the height of the impeller. A similar definition is used for the disc turbine:

$$Fl_1 = \frac{Q_1}{ND^3} = \frac{1}{ND^3}\int_{H-C-D/10}^{H-C+D/10} v(r = D/2)\pi D\,dz \quad (13)$$

The values of Fl_1 and Po are listed in Table 2. It should be noted that since the radial velocities could not be

Table 2. Power number, Flow number and Swirl number for the three impellers.

	Po	Fl_1	S
A315	0.76	0.74	0.31
PBT	1.55	0.81	0.52
DT	5.10	0.76	—

measured, the experimental k-values presented here were calculated as:

$$k = \tfrac{3}{4}(\overline{u'^2} + \overline{w'^2}) \tag{14}$$

The axial velocity profiles for the A315 is similar to the profile of the PBT, with low velocities near the centre and peaks in the velocities at about 0.4 D. The main difference between the two impellers lies in the tangential velocities. The A315 creates lower tangential velocities than the PBT. This can be seen from the Swirl number which is a measure for the ratio between the flux of angular momentum and the flux of axial momentum:

$$S = \frac{\int_0^{D/2} uwr^2\,\mathrm{d}r}{\tfrac{1}{2}D\int_0^{D/2} u^2 r\,\mathrm{d}r} \tag{15}$$

The Swirl numbers, as calculated from the experimental data, for the A315 and the PBT are listed in Table 2. The A315 converts less input energy in angular momentum than the PBT.

In all cases the turbulent kinetic energy k was prescribed according to the measurements, and the local energy dissipation rate ε was calculated, assuming that the turbulent length scale L_t:

$$L_t = \frac{k^{3/2}}{\varepsilon} \tag{16}$$

was proportional to the width W_b of the impeller blades:

$$\varepsilon = \frac{k^{3/2}}{\tfrac{1}{4}W_b} \tag{17}$$

The proportionality factor 1/4 was taken from Wu and Patterson[19].

The Computational Grid

The calculations were performed with the ASM on non-uniform three-dimensional grids. To check for possible grid dependency several grid sizes were tested: 50 × 25 × 20, 40 × 25 × 25, 52 × 27 × 17 and 56 × 35 × 11 grid nodes in (z, r, ϕ) coordinates. Here z denotes the distance from the liquid surface, r the radial distance from the centre and ϕ is the tangential coordinate, being 0° at the baffle.

Due to computational restrictions grids with more than 25000 grid nodes could not be tested.

The calculations were done for a 90° segment of the vessel with cyclic cells at $\phi = -45°$ and at $\phi = 45°$. The no-slip condition was applied using a wall law at the vessel walls, the bottom, the baffles and the impeller shaft. The liquid surface was treated as a free slip surface.

All results presented below were obtained with the ASM for the turbulent flow and with the Power-Law numerical scheme. Further details have been discussed elsewhere[3].

RESULTS CONCERNING THE MEAN FLOW

Disc Turbine

Figures 2a,b show the flow pattern for the disc turbine as calculated on a 3D grid with 50 × 25 × 20 nodes. Figure 2a shows the flow pattern in the plane midway between two baffles ($\phi = 45°$), whereas the velocity vectors in the plane just in front of a baffle ($\phi = -4°$) are shown in Figure 2b. In both planes the flow is characterized by two main circulation loops, one on each side of the impeller. It can be seen that at $\phi = -4°$ the centre of these loops lies more inward, and closer to the radial jet coming from the impeller than at $\phi = 45°$. To our knowledge this fact has not been reported before, but it shows that for an accurate numerical computation of the flow field full 3D-simulations are necessary.

Due to the fact that the turbine is mounted closer to the vessel bottom (at $C = 0.3\,T$) than to the liquid surface, the average axial liquid velocity at the top of the impeller was 1.4 times that at the bottom. This is illustrated in Figure 3 where the absolute values of the axial velocities on both sides of the turbine are plotted. This phenomenon probably results from the difference in friction above and below the impeller.

Figure 4 shows a comparison between the calculated axial velocity components and the measured axial velocities at different positions in the vessel. In general,

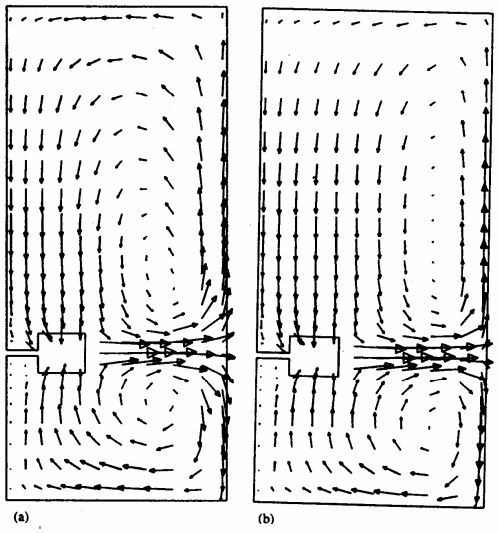

Figure 2. Velocity vectors for the disc turbine, in front of the baffle ($\phi = -4°$) and midway between the baffles ($\phi = 45°$).

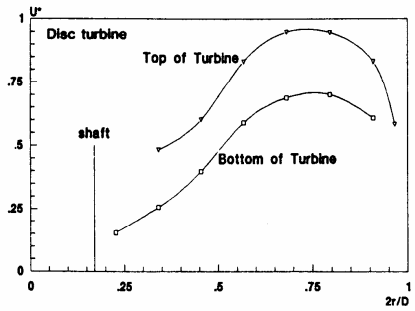

Figure 3. Absolute value of the axial velocity at the top of the turbine and at the bottom of the turbine.

the model predictions and the experimental data agree quite well thus giving confidence in the results for the mean velocities.

Axial Flow Impellers

The flow pattern calculated for the PBT turned out to be very sensitive to the exact baffle geometry. The computations presented here were done with 40 × 25 × 25 grid nodes.

Figures 5a,b,c show the flow pattern for a PBT with baffles mounted a small distance from the wall (0.023 *T*baffle-wall spacing). Figure 5a shows the flow pattern just in front of the baffle ($\phi = -2°$). In this plane the flow pattern consists of a large circulation loop, and a small recirculation loop below the impeller. A small distance behind the baffle ($\phi = +13°$) the flow pattern is approximately the same, although the centre of the large circulation loop is shifted slightly upwards, while the velocities are slightly smaller. The flow midway between the baffles ($\phi = 45°$) is different from the flow

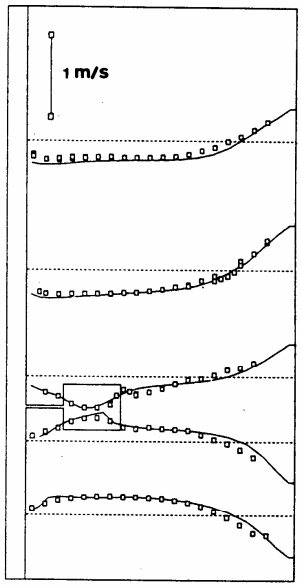

Figure 4. Comparison between predicted and measured axial velocities (□ experimental, ——— simulation) ($N = 3\ s^{-1}$; $\phi = 45°$).

pattern in front of the baffle. Now a small second recirculation loop has formed in the upper part of the vessel. The flow along the wall in the top of the vessel is directed downwards rather than upwards. In all planes a more or less dead zone with very small, partly upwards directed velocity vectors is found below the impeller.

The flow pattern with baffles mounted directly to the vessel wall, with zero spacing, is shown in Figures 6a,b,c. In front of the baffle (Figure 6a, $\phi = -2°$) the flow pattern consists of a large circulation loop, and a small recirculation loop below the impeller, approximately the

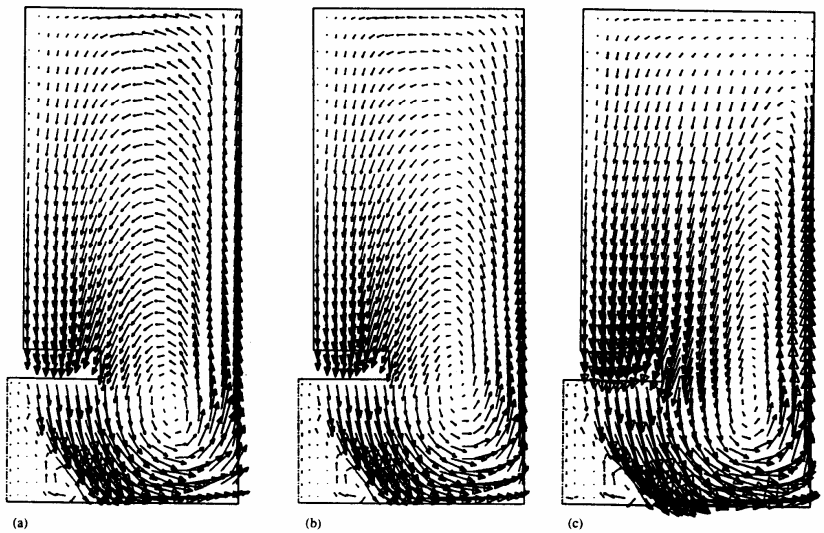

Figure 5. Velocity vectors for the pitched blade turbine with 0.023 *T* wall-baffle spacing, in front of baffle ($\phi = -2°$), behind baffle ($\phi = 13°$), midway baffles ($\phi = 45°$).

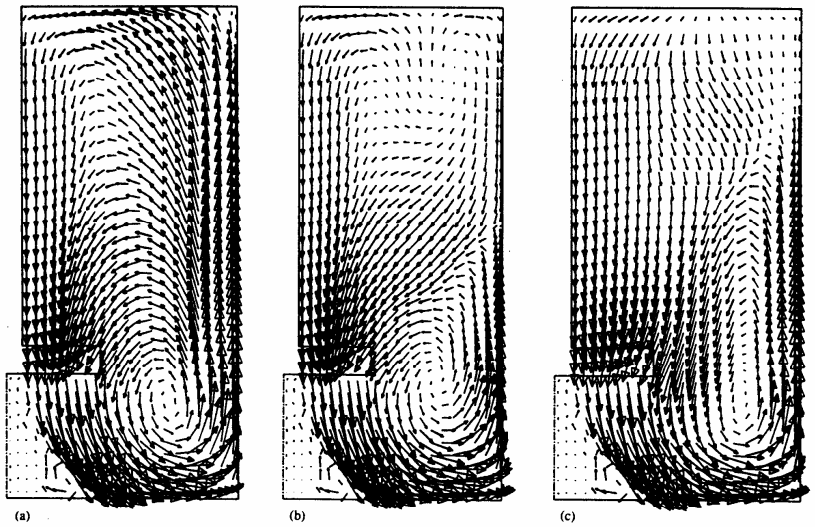

Figure 6. Velocity vectors for the pitched blade turbine with zero wall-baffle spacing, in front of baffle ($\phi = -2°$), behind baffle ($\phi = 13°$), midway baffles ($\phi = 45°$).

same as with 0.023 T baffle spacing. Just behind the baffle ($\phi = 13°$), however, a second circulation loop has formed in the upper part of the vessel. In this region the flow along the wall is directed downwards, rather than upwards. At $\phi = 45°$ this secondary loop is already much smaller.

Thus it can be concluded that both with zero baffle-wall spacing and with 0.023 T baffle-wall spacing, a second circulation loop is formed in the upper part of the vessel, but that the position and size of this loop are different. This can be explained by looking at the velocity vectors at two different heights in the vessel (Figures 7a,b and 8a,b). It can be seen that with zero baffle-wall spacing, a secondary circulation loop behind the baffle is found in the upper part of the vessel, with negative tangential velocities along the wall. With a small baffle wall spacing this does not occur, which explains why in this case the secondary circulation loop is much smaller.

The second recirculation loop extends about 50° away from the baffle. Bakker and Van den Akker[3] reported a value of 33°, but those calculations were done with 17 grid nodes in the tangential direction. Due to computational restrictions, it could not be tested whether grid independence has yet been achieved.

Figure 9 shows a comparison between calculated and measured profiles of the axial velocity at several positions in the vessel for 0.023 T baffle-wall spacing and a PBT. In general the model predictions agree quite well with the experimental data, except in the upper part of the vessel where according to the experimental data all mean velocities are directed downwards.

Thus it can be concluded that the predicted flow patterns are qualitatively correct, showing details not reported before in the literature, but that the quantitative accuracy in the upper part of the vessel could be improved even further.

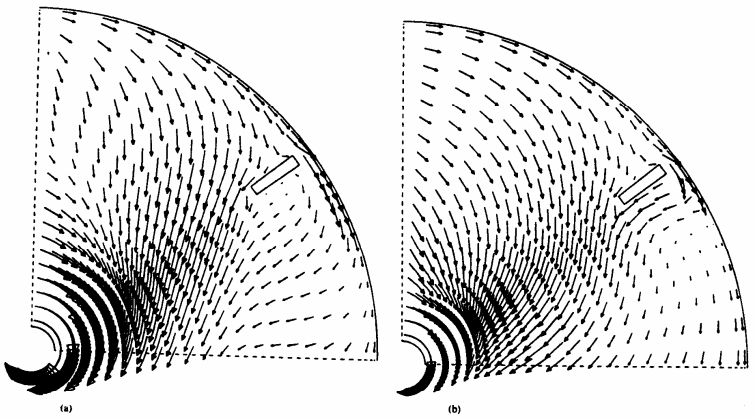

Figure 7. Velocity vectors for the pitched blade turbine, top view, 0.023 T baffle-wall spacing, $z/H = 0.28$ (left) and $z/H = 0.66$ (right).

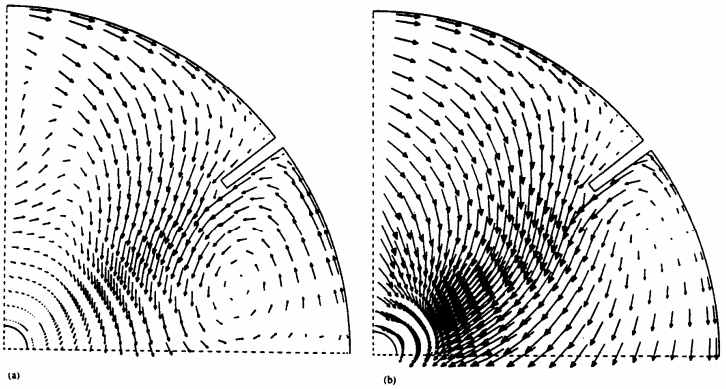

Figure 8. Velocity vectors for the pitched blade turbine, top view, zero baffle-wall spacing, $z/H = 0.28$ (left) and $z/H = 0.66$ (right).

RESULTS CONCERNING THE TURBULENCE

Turbulence Distribution

To validate the predicted turbulence properties, experimentally determined profiles of RMS(u') (RMS = Root Mean Square) and computed profiles were compared. Figure 10 shows the comparison for the A315, as calculated with the aid of the ASM. The predicted values of RMS(u') compare better with the measured values in the regions near the baffles than in the regions above and below the impeller. This might be due to the fact that the flow pattern as induced by the rotating impeller will contain periodic high frequency velocity fluctuations, a phenomenon called pseudo-turbulence. These fluctuations will increase the measured values of RMS(u') in the inflow and outflow of the impeller, but may well be dampened out near the baffles. As a result, the predictions for RMS(u') will be more accurate near the baffles.

The values of k which are prescribed in the outflow of the impeller contain these velocity periodic velocity fluctuations. However, RMS(u') is still under predicted near the vessel bottom, in the outflow of the impeller. This is probably due to the fact that the pseudo-turbulence and the real turbulence have different dissipation rates. It may be worth investigating whether the use of the two-scale turbulence model proposed by Placek *et al.* (1986), with separate equations for the turbulent kinetic energy and the kinetic energy of the pseudo turbulence, gives better results.

The anisotropy of the turbulence is illustrated by Figure 11. This graph shows a comparison between the predicted values of RMS(u'), RMS(v') and RMS(w') together with the measured values of RMS(u') and the

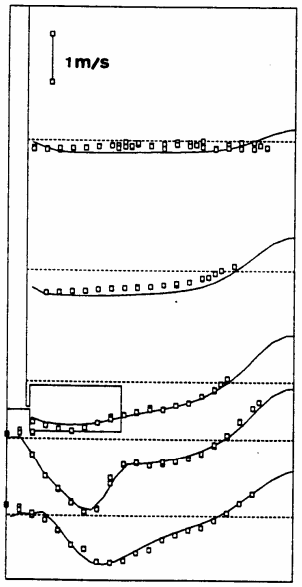

Figure 9. Comparison between predicted axial velocities and measured axial velocities, pitched blade turbine (□ experimental, ——— simulation) ($N = 6\ s^{-1}$; $\phi = 45°$).

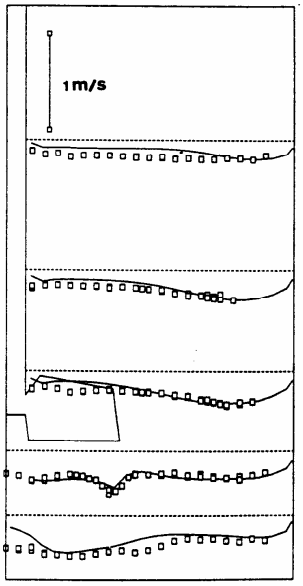

Figure 10. Comparison between predicted and measured RM (u'), A315. (□ experimental and ——— simulation) ($N = 6\ s^{-1}$; $\phi = 45°$).

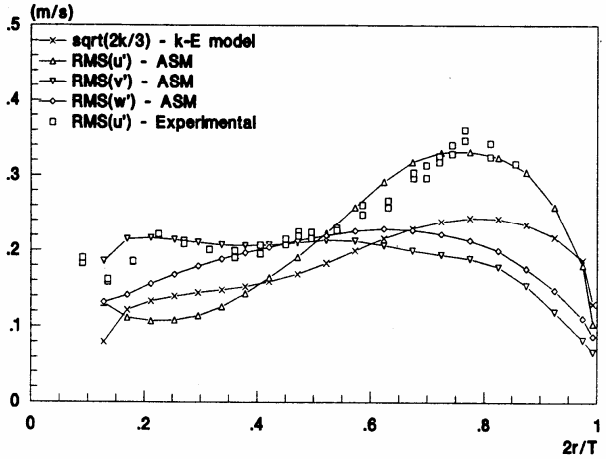

Figure 11. Experimental data for RMS(u'), predicted data for RMS(u'), RMS(v') and RMS(w') with ASM and $(2k/3)^{1/2} \approx$ RMS(u') with $k-\varepsilon$ (just above A315, $z/H = 0.64$; $\phi = 45°$; $N = 6\ s^{-1}$).

value of $(2k/3)^{1/2}$ as predicted with the k-ε model. The value of $(2k/3)^{1/2}$ is a measure of RMS(u') as predicted by the k-ε model. It is clear that the values of RMS(u') as predicted by the ASM compare better with the experimental data than the value of $(2k/3)^{1/2}$ as predicted by the isotropic k-ε model. Further, there are large differences between the values of RMS(u'), RMS(v') and RMS(w'), thus showing the need for anisotropic turbulence models.

Contours of equal turbulent kinetic energy and dissipation rate, as calculated with the ASM, are plotted in Figures 12 and 13 for both the disc-turbine and the PBT. It can be seen that in both cases the highest turbulence intensities are found in the outflow of the impellers, and that both k and ε are much lower in the bulk of the vessel.

With the PBT a region of high values of both k and ε is found near the baffles, above the impeller. This is probably due to the large velocity gradients near the centre of the main circulation loop and the interaction with the secondary flow loop in the top of the vessel. Large velocity gradients lead to an increased production P_k of turbulent kinetic energy and production of Reynolds stresses. (Equations (8), (10)). As a consequence the production P_ε of ε also increases, since in the model equations it is assumed that P_ε is proportional to P_k:

$$P_\varepsilon \sim \frac{\varepsilon}{k} P_k \tag{18}$$

Energetic Efficiency

The power consumption P of an impeller is given by:

$$P = Po\rho N^3 D^5 \tag{19}$$

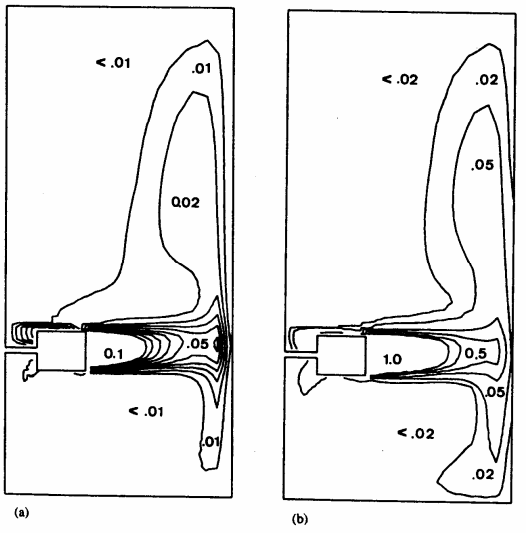

Figure 12. Contours of constant k (m^2s^{-2}) and ε (m^2s^{-3}) for the disc turbine (3 Hz), numbers denote minimum values in areas enclosed by contours.

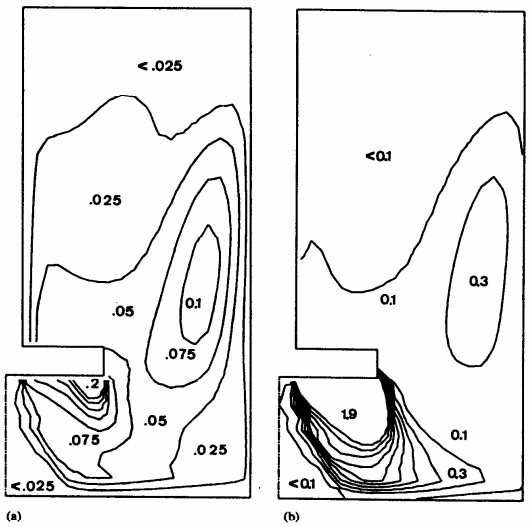

Figure 13. Same as Figure 17 but now for the pitched blade turbine (6 Hz).

Here Po denotes the so-called power number which, for a given vessel geometry, is a function of impeller type only. A significant part of the energy input is dissipated in the impeller swept volume V_{imp} rather than in the liquid bulk. Since the local mixing in the liquid bulk may be determined by the local turbulence intensity, it is necessary to have an estimation of the fraction of the total energy input which is dissipated in the liquid bulk. Therefore the energetic efficiency η_e can be defined as:

$$\eta_e = 1 - \frac{V_{imp}\langle\varepsilon_{imp}\rangle\rho}{P} \tag{20}$$

Here $\langle\varepsilon_{imp}\rangle$ denotes the average energy dissipation rate per unit mass in the impeller zone. The energetic efficiency is difficult to measure since it requires measuring local values of ε. Therefore it is not surprising that different authors present different values for η_e. Experimental studies with the disc turbine resulted in values ranging from 40% to 70% (see the review by Ranade and Joshi[12]). This means that between 30% and 60% of the total energy input is dissipated in the impeller swept volume, which makes up only 1.2% of the total volume, thus leading to extremely large values of $\langle\varepsilon_{imp}\rangle$. According to the experimental data from Ranade and Joshi[10,11] the energetic efficiency for a pitched blade turbine ranges from 53% to 78% depending on blade width, impeller to bottom clearance and D/T ratio. For the A315 no data regarding η_e are available in the open literature.

It should be noted that η_e is not the same as the pumping efficiency defined by Bakker and Van den Akker[20]. The pumping efficiency η_p is the fraction of the energy which is used in the main flow, and can thus be defined as the ratio of the gain in enthalpy of the fluid, ΔpQ_1, to the power input P by the impeller. The pressure rise Δp over the impeller as determined by, among other things, rotational speed N and impeller geometry is converted into velocity head of a circulatory flow:

$$\Delta p = K_w \tfrac{1}{2}\rho_1\overline{v^2} \sim \rho_1 \frac{Q_1^2}{T^2} \tag{21}$$

The proportionality constant K_w depends on the vessel geometry only and is not known in general. By using Po and Fl_1 the following relation can be found:

$$\eta_p = \Delta p \frac{Q_1}{P} \sim \left(\frac{D}{T}\right)^4 \frac{Fl_1^3}{Po} \tag{22}$$

In general, the pumping efficiency will be lower than the energetic efficiency since the energy which is put into the generation of turbulent kinetic energy by the impeller and in trailing vortices shed from the impeller blades is included in the energetic efficiency but not in the pumping efficiency.

The predicted values for η_e both according to the calculations with the k-ε model and the ASM are listed in Table 3. It can be seen that with the DT the predicted value of η_e compares well with the literature values, provided that the ASM is used. With the k-ε model, the predicted energy dissipation rates are significantly lower than with the ASM.

With the PBT the predicted η_e is on the low side, which might be due to a too low predicted ε as a result of not taking the pseudo turbulence into account. The predicted η_e is higher for the A315 than for the PBT as a result of the profiled blades.

Table 3. Predicted values of η_e with k-ε and ASM.

	$\eta_e(k-\varepsilon)$	η_e(ASM)	Literature
A315	48%	57%	—
PBT	38%	45%	53%–78%
DT	45%	53%	40%–70%

STABILITY OF THE MEAN FLOW

All the calculations have been done assuming a steady state flow with normally distributed turbulent velocity fluctuations. This assumption turns out not always to be valid. Figure 14a shows an experimentally determined velocity distribution for the PBT at $z/T = 0.45$ and at $2r/T = 0.88$, just above the impeller near the vessel wall. In this region the measured velocities are indeed Gaussian distributed. In the upper part of the vessel, at $z/H = 0.25$ at $2r/T = 0.13$, (Figure 14b), however, the measured liquid velocities turn out to have a bimodal distribution. This suggests that the flow in this region is bistable, and that it oscillates periodically. It would be

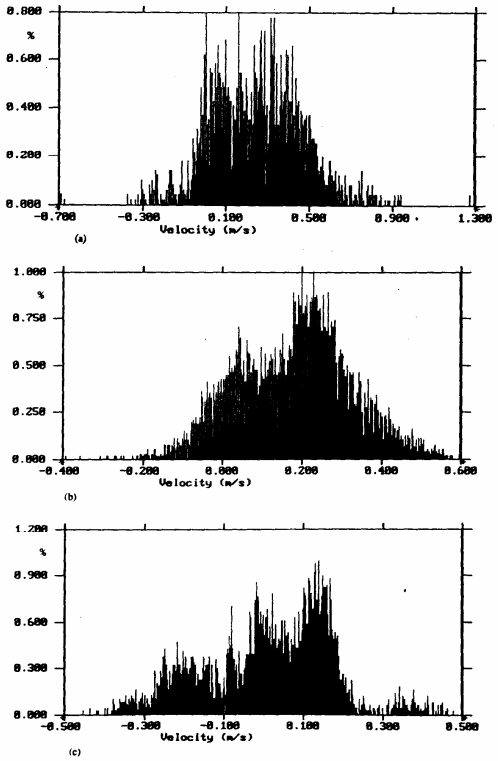

Figure 14. Measured u-distribution: PBT; $\phi = 45°$; (a) ($z/H = 0.45$, $2r/T = 0.88$); (b) ($z/H = 0.25$, $2r/T = 0.13$); (c) ($z/H = 0.10$, $2r/T = 0.88$).

interesting to see whether it is possible to resolve this oscillating behaviour by performing time-dependent calculations. Unfortunately, due to computational restrictions this could not be tested.

Close to the liquid surface (Figure 14c, $z/T = 0.1$, $2r/T = 0.88$) the velocity distribution has three peaks, at a negative axial velocity, near zero, and at a positive axial velocity. This is probably a result of waves, running at the liquid surface. Thus, it is unlikely that any turbulence model will give a realistic picture of the flow in this part of the vessel.

Although skewed velocity distributions were sometimes observed with the DT and the A315, bimodal and trimodal distributions were only observed with the PBT in the upper part of the vessel. This may be related to a higher strength of the swirl in (the upper part of) the vessel with the PBT, see Table 2. These deviations from Gaussian turbulence might to some extent be responsible for the differences between the measured velocity and turbulence data and the predicted data in this region, as compared in Figures 9 and 11. Whether this problem can be solved by performing transient calculations is not clear.

CONCLUSIONS

Both two-dimensional computations and three-dimensional computations of the single-phase flow in stirred vessels have been performed. In general it can be concluded that the flow pattern in stirred vessels is fully three-dimensional, exhibiting secondary recirculation loops and unexpected features not recognized before.

With the disc turbine it was found that the position of the centre of the two main circulation loops is a function of the tangential coordinate ϕ. The predicted flow patterns for the disc turbine were found to match quite well with the experimental data. Further, it was found that when the turbine is mounted closer to the vessel bottom than to the liquid surface ($C/T = 0.3$), the axial velocities at the top of the impeller are about 1.4 times those at the bottom of the impeller.

The flow pattern of the axial flow impellers turned out to be sensitive to the exact baffle configuration. Both with zero baffle-wall spacing and with 0.023 T baffle-wall spacing a second circulation loop in the upper part of the vessel is formed. The exact size and position of this loop is determined by the baffle geometry. The existence of this secondary loop is proven by experimental data. With two-dimensional simulations this loop was not found, thus clearly showing the need for three-dimensional simulations. In general, the fluid flow predictions and the experimental data match quite well, although in the upper part of the vessel the quantitative accuracy could be improved even further.

In the upper part of the vessel bimodal and trimodal velocity distributions were measured. This shows that the assumption of steady state flow with normally distributed turbulent velocity fluctuations is not always valid in this region. It might be necessary to perform transient flow field computations to reproduce these phenomena.

In case of a zero baffle-wall spacing a secondary circulation loop behind the baffle was found in the upper part of the vessel, with negative tangential velocities.

The tangential velocities in the outflow of the A315 are 50% lower than with the PBT leading to an increased pumping efficiency.

For all impellers the turbulence distribution is far from homogeneous, with high turbulence intensities in the outflow of the impellers and in the centres of the main circulation loops. It was found that the predicted overall energy dissipation rates compare reasonably with power measurements, but that with the ASM the predicted energy dissipation rates are about 15% higher than with the k-ε model. Thus for the prediction of turbulent mixing, the use of the ASM is necessary.

The use of single-phase flow pattern simulations as a basis for a description of the mixing processes in a stirred tank, can only be successful if the computations are done on a three-dimensional grid, with the aid of an anisotropic turbulence model.

CFD is a useful tool in the analysis of the flow in stirred mixing vessels. The computations in this paper have shown that it is even possible to discover flow features which otherwise would require very extensive sets of LDV measurements. A disadvantage at the present stage is that LDV data are required for prescribing impeller boundary conditions. Thus further research should concentrate on the development of accurate impeller models.

NOMENCLATURE

c_μ	model constant
c_ε	model constant
$c_{\varepsilon 1}$	model constant
$c_{\varepsilon 2}$	model constant
c_1	model constant
c_2	model constant
C	impeller to bottom clearance
D	impeller swept diameter
Fl_l	impeller pumping number
Fl_g	gas flow number
H	liquid height
$\bar{\bar{I}}$	unit tensor
k	turbulent kinetic energy per fluid mass
K_w	friction coefficient
L_t	turbulent length scale
N	impeller rotational speed
p	pressure
P	power consumption
$\bar{\bar{P}}$	Reynolds stress production tensor
P_k	production of k by interaction with mean strain rate
Po	impeller power number
Q_l	liquid flow rate
r	radial coordinate (outwards positive)
S	swirl number
T	vessel diameter
u	axial velocity (downwards positive)
$\bar{u}$	time-averaged velocity vector
$\bar{u}'$	fluctuating component of the velocity vector
v	radial velocity (outwards positive)
$\langle v_{ax} \rangle$	average axial liquid velocity out of the impeller plane
V	volume
V_{imp}	impeller swept volume
w	tangential velocity (with impeller positive)
W	baffle width
W_b	width of impeller blade
z	axial coordinate, 0 at liquid surface

Greek Symbols

ε	turbulent energy dissipation rate density
ε_{imp}	turbulent energy dissipation rate density in impeller region
$\langle\varepsilon\rangle$	average energy dissipation rate density
ϕ	tangential coordinate (0° at baffle)
η	dynamic viscosity
η_e	energetic efficiency
η_p	pumping efficiency
ν	kinematic viscosity
ν_t	turbulent viscosity
ρ	density
σ_k	model constant
σ_ε	model constant

Abbreviations

ASM	Albebraic Stress Model
CFD	Computational Fluid Dynamics
DT	Disc Turbine (Rushton Turbine)
LDV	Laser Doppler Velocimetry
PBT	Downwards pumping Pitched Blade Turbine, 6 blades at 45° blade angle
RMS	Root Mean Square
RSM	Reynolds Stress Model

REFERENCES

1. Bakker, A. and Van den Akker, H. E. A., 1994, Gas–liquid contacting with axial flow impellers, *Trans IChemE Part A*, 72: 573–582.
2. Bakker, A., 1992, Hydrodynamics of stirred gas-liquid dispersions, PhD Thesis, (Delft University of Technology, The Netherlands).
3. Bakker, A. and Van den Akker, H. E. A., 1991, A computational study on dispersing gas in a stirred reactor *Proc 7th Eur Conf Mixing*, Brugge, Belgium, September 18–20, 199–207.
4. Harvey, P. S. and Greaves, M., 1982a, Turbulent flow in an agitated vessel; Part 1: A predictive model, *Trans IChemE*, 60: 195–200.
5. Harvey, P. S. and Greaves, M., 1982b, Turbulent flow in an agitated vessel; Part 2: Numerical simulation and model predictions, *Trans IChemE*, 60: 201–210.
6. Placek, J. and Tavlarides, L. L., 1985, Turbulent flows in stirred tanks; Part 1: Turbulent flow in the turbine impeller region, *AIChE Journal*, 31: 1113–1120.
7. Placek, J., Tavlarides, L. L., Smith, G. W. and Fort, I., 1986, Turbulent flows in stirred tanks; Part 2: A two scale model of turbulence, *AIChE Journal*, 32: 1771–1785.
8. Pericleous, K. A. and Patel, M. K., 1987, The modelling of tangential and axial agitators in chemical reactors, *Physico Chemico Hydrodynamics*, 8: 105–123.
9. Middleton, J. C., Pierce, F. and Lynch, P. M., 1986, Computations of flow fields and complex reaction yield in turbulent stirred reactors and comparison with experimental data *Chem Eng Res Des*, 64: 18–22.
10. Ranade, V. V. and Joshi, J. B., 1989a, Flow generated by pitched blade turbines 1: Measurements using laser-doppler anemometer, *Chem Eng Comm*, 81: 197–224.
11. Ranade, V. V., Joshi, J. B. and Marathe, A. G., 1989b, Flow generated by pitched blade turbines 2: Simulation using k-ε model, *Chem Eng Comm*, 81: 225–248.
12. Ranade, V. V. and Joshi, J. B., 1990a, Flow generated by a disc-turbine Part 1: Experimental, *Trans IChemE*, 60: 19–33.
13. Ranade, V. V. and Joshi, J. B., 1990b, Flow generated by a disc-turbine Part 2: Mathematical modelling and comparison with experimental data *Trans IChem E*, 60: 34–50.
14. Hutchings, B. J., Weetman, R. J. and Patel, B. R., 1989, Computation of flow fields in mixing tanks with experimental verification, *ASME Annual Meeting, San Francisco, December 10–15.*
15. Kresta, S. M. and Wood, P. E., 1991, Prediction of the three-dimensional turbulent flow in stirred tanks, *AIChE Journal*, 37: 448–460.
16. Van't Riet, K., Bruijn, W. and Smith, J. M., 1976, Real and pseudo turbulence in the discharge stream from a Rushton turbine, *Chem Eng Sci*, 31: 407–412.
17. Rodi, W., 1980, *Turbulence Models and Their Application in Hydraulics—A State of the Art Review* (International Association for Hydraulic Research, Delft, The Netherlands).
18. Boysan, F., 1984, Mathematical modelling of cyclone separators *Selected Topics in Two-Phase Flow, Lecture Series no. 9, Trondheim, May 25.*
19. Wu, H. and Patterson, G. K., 1989, Laser-Doppler measurements of turbulent flow parameters in a stirred mixer, *Chem Eng Sci*, 8: 244–253.
20. Bakker, A. and Van den Akker, H. E. A., 1990, The use of profiled axial flow impellers in gas-liquid reactors, *Proc Fluid Mixing IV, Bradford UK, September 11–13 1990, IChemE. Symposium Series* No 121: 153–166.

ACKNOWLEDGEMENT

These investigations were financially supported by the Netherlands Technology Foundation (STW, project DTN 40.0566).

The authors are grateful to J. van Raamt for his assistance in performing the Laser-Doppler experiments.

ADDRESS

Correspondence concerning this paper should be addressed to Dr A. Bakker, Chemineer Inc, 5870 Poe Avenue, Dayton, OH 45414, USA.

The manuscript was communicated via our International Editor for Continental Europe, Dr A. D. Barber. It was received 23 October 1991 and accepted for publication after revision 17 August 1993.